# Fabrication of three-dimensional micro-photonic structures on the tip of optical fibers using SU-8

**Henry E. Williams,[1] Daniel J. Freppon,[1] Stephen M. Kuebler,[1,2,3,*] Raymond C. Rumpf,[4] and Marco A. Melino[2]**

[1]*Chemistry Department, University of Central Florida, Orlando, FL 32816 USA*
[2]*CREOL, The College of Optics and Photonics, University of Central Florida, Orlando, FL 32816 USA*
[3]*Physics Department, University of Central Florida, Orlando, FL 32816 USA*
[4]*EM Lab, W. M. Keck Center for 3D Innovation, The University of Texas at El Paso, El Paso, TX 79968 USA*
[*]*stephen.kuebler@ucf.edu*

**Abstract:** A method is reported for fabricating truly three-dimensional micro-photonic structures directly onto the end face of an optical fiber using the cross-linkable resist SU-8. This epoxide-based material is well suited for micro-device fabrication because it is photo-processed as a solid and the cross-linked material is mechanically robust, chemically resistant, and optically transparent. Yet, procedures commonly used to process SU-8, particularly spin-coating, are impractical when the intended fabrication substrate is the end-face of an optical fiber. A melt-reflow process was developed to prepare optical fibers having SU-8 resin deposited at controlled thickness on the fiber end-face. Multi-photon direct laser writing was then used to fabricate various refractive lenses, a compound lens system, and a woodpile photonic crystal within the resin on the end-face of the optical fiber. Data are presented that show how the refractive lenses can be used to alter the output of the optical fiber. This work opens a new path to low-profile integrated photonic devices.



**OCIS codes:** (350.4238) Nanophotonics and photonic crystals; (160.3918) Microstructure fabrication; (350.3390) Laser materials processing.

## References and links

1. F. Schiappelli, R. Kumar, M. Prasciolu, D. Cojoc, S. Cabrini, R. Proietti, V. Degiorgio, and E. Di Fabrizio, "Design and fabrication of diffractive optical element-microlens with continuous relief fabricated on-top of optical fibre," Jpn. J. Appl. Phys. **43**(6B), 3772–3778 (2004).
2. H. T. Yan, M. Wang, Y. X. Ge, and X. X. Chen, "The method and simulation of the three-dimensional colloidal crystal growth on the end face of optical fiber," in *International Conference on Smart Materials and Nanotechnology in Engineering,* S. Du, J. Leng, and A. K. Asundi, eds. (SPIE, Harbin, China, 2007), pp. 64234C–64231 - 64234C–64236.
3. T. Sherwood, A. C. Young, J. Takayesu, A. K. Y. Jen, L. R. Dalton, and A. Chen, "Microring resonators on side-polished optical fiber," IEEE Photon. Technol. Lett. **17**(10), 2107–2109 (2005).
4. G. Cojoc, C. Liberale, P. Candeloro, F. Gentile, G. Das, F. De Angelis, and E. Di Fabrizio, "Optical micro-structures fabricated on top of optical fibers by means of two-photon photopolymerization," Microelectron. Eng. **87**(5-8), 876–879 (2010).
5. K. Y. Lee, N. LaBianca, S. A. Rishton, S. Zolgharnain, J. D. Gelorme, J. Shaw, and T. H.-P. Chang, "Micromachining applications of a high resolution ultrathick photoresist," J. Vac. Sci. Technol. B **13**(6), 3012–3016 (1995).
6. H. Lorenz, M. Despont, N. Fahrni, N. LaBianca, P. Renaud, and P. Vettiger, "SU-8: a low-cost negative resist for MEMS," J. Micromech. Microeng. **7**(3), 121–124 (1997).
7. Y.-S. Chen, A. Tal, and S. M. Kuebler, "Route to three-dimensional metallized micro-structures using cross-linkable epoxide SU-8," Chem. Mater. **19**(16), 3858–3860 (2007).
8. S. M. Kuebler and M. Rumi, "Nonlinear optics - applications: three-dimensional microfabrication," in *Encyclopedia of Modern Optics*, R. D. Guenther, D. G. Steel, and L. Bayvel, eds. (Elsevier, Oxford, 2004), pp. 189–206.
9. T.-C. Poon and T. Kim, *Engineering Optics with MatLab* (World Scientific Publishing Co., Hackensack, NJ, 2006).
10. D. Nilsson, S. Balslev, M. M. Gregersen, and A. Kristensen, "Microfabricated solid-state dye lasers based on a photodefinable polymer," Appl. Opt. **44**(23), 4965–4971 (2005).

#153624 - $15.00 USD Received 31 Aug 2011; revised 14 Oct 2011; accepted 16 Oct 2011; published 27 Oct 2011

11. K. K. Seet, V. Mizeikis, S. Juodkazis, and H. Misawa, "Spiral three-dimensional photonic crystals for telecommunications spectral range," Appl. Phys., A Mater. Sci. Process. **82**(4), 683–688 (2006).
12. J. Zhang, K. L. Tan, G. D. Hong, L. J. Yang, and H. Q. Gong, "Polymerization optimization of SU-8 photoresist and its applications in microfluidic systems and MEMS," J. Micromech. Microeng. **11**(1), 20–26 (2001).
13. Z. Cui, D. W. K. Jenkins, A. Schneider, and G. McBride, "Profile control of SU-8 photoresist using different radiation sources," Proc. SPIE 4407, 119–125 (2001).
14. L. Singleton, A. L. Bogdanov, S. S. Peredkov, O. Wilhelmi, A. Schneider, C. Cremers, S. Megtert, and A. Schmidt, "Deep X-ray lithography with the SU-8 resist," Proc. SPIE 4343, 182–192 (2001).
15. V. Nazmov, E. Reznikova, J. Mohr, A. Snigirev, I. Snigireva, S. Achenbach, and V. Saile, "Fabrication and preliminary testing of X-ray lenses in thick SU-8 resist layers," Microsyst. Technol. **10**(10), 716–721 (2004).
16. R. G. Denning, C. F. Blanford, H. Urban, H. Bharaj, D. N. Sharp, and A. J. Turberfield, "The control of shrinkage and thermal instability in SU-8 photoresists for holographic lithography," Adv. Funct. Mater. **21**(9), 1593–1601 (2011).
17. C. Becnel, Y. Desta, and K. Kelly, "Ultra-deep X-ray lithography of densely packed SU-8 features: II. Process performance as a function of dose, feature height and post exposure bake temperature," J. Micromech. Microeng. **15**(6), 1249–1259 (2005).
18. C. Becnel, Y. Desta, and K. Kelly, "Ultra-deep X-ray lithography of densely packed SU-8 features: I. An SU-8 casting procedure to obtain uniform solvent content with accompanying experimental results," J. Micromech. Microeng. **15**(6), 1242–1248 (2005).
19. K. S. Lee and F. S. Barnes, "Microlenses on the end of single-mode optical fibers for laser applications," Appl. Opt. **24**(19), 3134–3139 (1985).
20. K. S. Lee, "Focusing characteristics of a truncated and aberrated Gaussian beam through a hemispherical microlens," Appl. Opt. **25**(20), 3671–3676 (1986).
21. M. Born and E. Wolf, *Principles of Optics,* 6th ed. (Cambridge University Press, Cambridge, 1997).

## 1. Introduction

The continuing transition from electronic to photonic telecommunications, information processing, and sensing has been enabled in large part by the inherent advantages of optical waveguiding offered by optical fibers. Further advances are expected to make increasing use of truly integrated photonic devices that do not require opto-electro-optical interconversion or bulky interconnects. To facilitate such advances, new approaches and material systems are needed for creating two- and three-dimensional integrated photonic devices, particularly those that can leverage existing technologies in fiber optic and electro-optic device fabrication. Numerous approaches have been reported for integrating refractive and diffractive optical devices with optical fibers. Few, however, are suitable for fabrication of arbitrary three-dimensional optical elements directly onto optical fibers [1,2]. Multi-photon direct laser writing (DLW) has been used to fabricate functional optical elements on side-polished optical fibers [3] and cleaved end faces [4] using liquid photopolymer resins.

SU-8 is a high-performance multi-functional epoxide that is increasingly employed for fabricating micro-electromechanical systems (MEMS), optical MEMS (OMEMS), and integrated photonic devices. SU8 is well suited for micro-fabrication because the material is photo-patterned as a solid, and the cross-linked material is mechanically robust, chemically resistant, and optically transparent [5,6]. The surface of processed SU-8 can also be chemically functionalized to imbue a structure with targeted physical and chemical properties [7]. SU-8 is most commonly processed as a viscous solution that is spin-coated onto a substrate then baked to remove solvent. The resulting solid film is irradiated in the target pattern, baked to activate acid-catalyzed cross-linking, and developed in a solvent that removes the unexposed material, yielding the final structure. These processing steps, particularly spin coating and subsequent bake-out, make it difficult to use SU-8 as a medium for fabricating optical elements onto optical fibers.

#153624 - $15.00 USD Received 31 Aug 2011; revised 14 Oct 2011; accepted 16 Oct 2011; published 27 Oct 2011

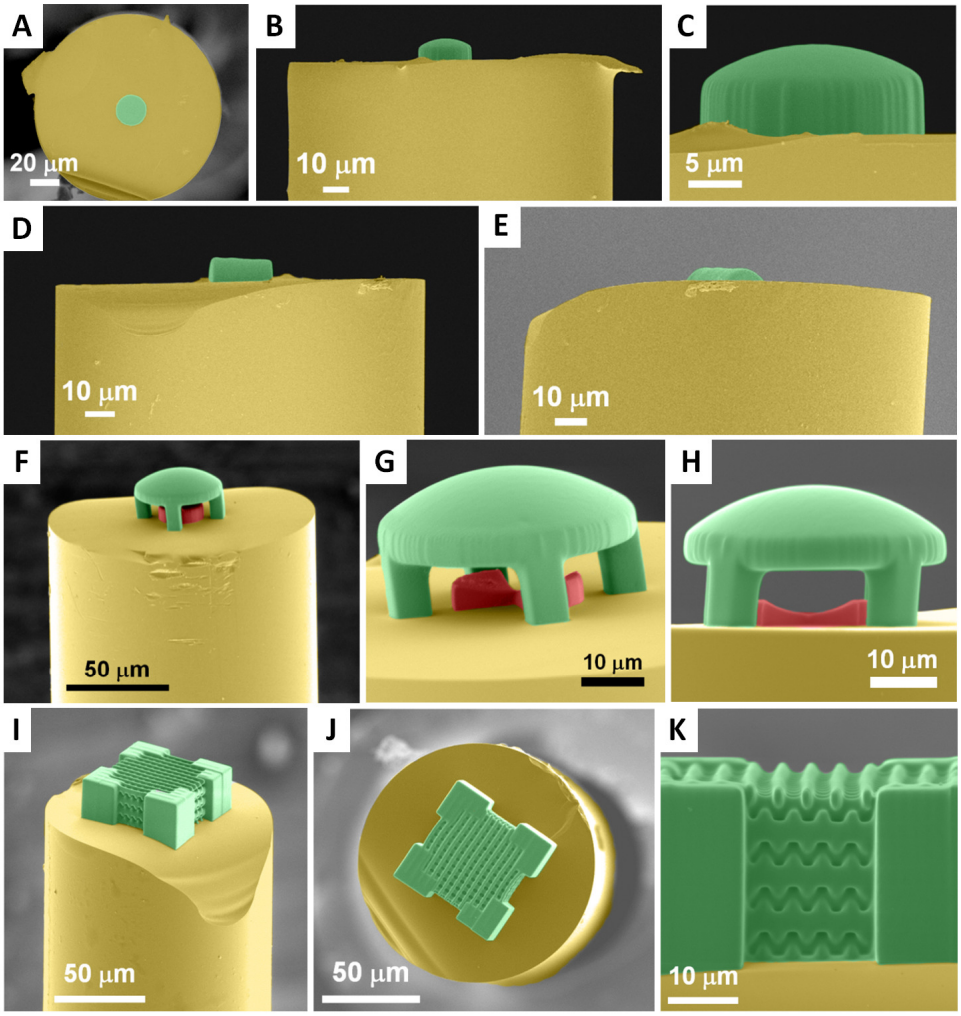


Fig. 1. False-color SEM images of micro-structures created on the end of an optical fiber by DLW in SU-8 resin. (**A C**) Plano-convex lens having radius of curvature $R$ = + 18.3 μm viewed (A) down the fiber axis and (B, C) from the side. (**D, E**) Cylindrical lens having $R$ = + 15.7 μm. (**F**) - (**H**) Compound micro-optic system consisting of a suspended plano-convex lens having $R$ = + 29.5 μm and a smaller plano-concave lens in contact with the fiber end-face having $R$ = –23.1 μm. For the structure shown in (G) and (H), only the first and third quandrants of the negative lens were fabricated so the internal curvature could be seen clearly. (**I K**) A woodpile face-centered tetragonal photonic crystal.

This report describes a process that enables SU-8 to be used for fabrication of micro-optical components directly onto the end face of an optical fiber by DLW. In this approach, solvent-free SU-8 resin is first obtained by heating *in vacuo* to remove volatiles. The resulting resin solids are then melt-reflowed around the optical fiber in a mould integrated into a sample mount. Upon cooling, the solidified resin immobilizes the optical fiber, so the entire sample mount can be affixed to the optical system for multi-photon patterning. Using this approach, a wide range of refractive and diffractive structures can be integrated onto an optical fiber, as shown in Fig. 1. Optical fibers bearing conventional refractive elements can be readily prepared, including radially symmetric convex and concave lenses (Figs. 1A – 1C) and cylindrical lenses (Figs. 1D – 1E). Truly three-dimensional structures with complex topology and undercut can also be fabricated, such as multi-lens systems (Figs. 1F – 1H) and "woodpile" photonic crystals (Figs. 1I – 1K), that would be impossible to create by other

#153624 - $15.00 USD Received 31 Aug 2011; revised 14 Oct 2011; accepted 16 Oct 2011; published 27 Oct 2011

existing methods. The remainder of this work provides a detailed description and characterization of the process and some optical characterization of refractive devices prepared using the approach.

## 2. Experimental

### *2.1. Isolation of SU-8 resin solids*

SU-8 2075 (MicroChem Corporation) is supplied as a clear viscous liquid consisting of SU-8 (an epoxide-functionalized bisphenol A oligomer, CAS 28906-96-9, 70 wt-%), two triarylsulfonium hexafluoroantimonate photoacid generators (CAS 89452-37-9 and 71449-78-0, 3.5 wt-% total), cyclopentanone solvent (CAS 120-92-3), and propylene carbonate (CAS 108-32-7), which functions as a plasticizer. A 50 mL round bottom flask was charged with 10 mL of SU8 2075 and a magnetic stir bar. The flask was affixed to a rotary evaporator and immersed in an oil bath heated to 95 °C. The pressure in the flask was reduced gradually to remove solvent, without foaming. This was continued until the pressure could be maintained at or below 9 Torr for at least 30 minutes, at which point the majority of the volatiles had been removed. The round bottom flask was connected to a vacuum manifold and heating was continued for 1 - 14 hours with full vacuum applied (< 0.5 Torr). The molten resin was then poured onto a clean glass plate and allowed to cool. The resulting solids were broken into *circa* 2-mm pieces and stored until needed for melt-reflow.

### *2.2. Characterization of vacuum-baked SU-8 resin*

Proton nuclear magnetic resonance spectroscopy ($^1$H NMR) was used to quantify the solvent content of SU-8 resin as a function of time heated *in vacuo*. This approach was chosen in preference to gravimetric methods because it is more accurate for low solvent levels, and it is not subject to error resulting from mass transfer loss during handling. All samples were studied as solutions in deuterated chloroform ($CDCl_3$) using tetramethylsilane as an internal reference. By comparing spectra obtained for SU-8 2075 resin, pure SU-8 oligomer, and cyclopentanone solvent, it was determined that peaks appearing in the region 6.4 - 7.2 ppm (complex multiplet) can be assigned to aromatic protons on SU-8, and those appearing in the range 1.8 - 2.3 ppm (pair of roofed multiplets) can be assigned to the solvent. A series of $^1$H NMR spectra were recorded for SU-8 dissolved in varying amounts of cyclopentanone to generate a calibration curve that related integrated areas of SU-8 and solvent peaks to their corresponding relative masses. Samples of vacuum-baked resin were analyzed as 5-mg solutions in $CDCl_3$, and the integrated solvent and SU-8 peak areas were converted to relative masses using the calibration curve. The solvent content of the processed resin could then be expressed for each sample as

$$\text{solvent mass-percent} \equiv \frac{\text{mass of cyclopentanone}}{\text{mass of SU8 oligomer} + \text{mass of cyclopentanone}} \times 100\%.$$

The definition does not account for the mass of the nonvolatile photoacid generator or the propylene carbonate plasticizer. But values of solvent mass-percent calculated in this way will be comparable to those determined gravimetrically because the oligomer and solvent constitute roughly 90% of the resin mass as-supplied.

### *2.3. Preparation of optical fiber for direct laser writing*

A mount was constructed (Fig. 2A) that enables an optical fiber to be affixed and positioned within a plug of vacuum-baked SU-8 resin at a targeted depth, then transferred as a unit onto a three-axis nano-positioner for DLW. The mount consists of a fiber chuck attached to a single-axis translation stage positioned above a clear-bored aluminum plate. The aluminum plate serves as a mould for casting vacuum-baked resin around the fiber.

Micro-optical structures were fabricated onto single-mode fibers (Nufern/ThorLabs 630 HP; core diameter = 3.3 ± 0.1 μm; at $\lambda_0$ = 633 nm, $n_{core}$ = 1.463, $n_{clad}$ = 1.457). A 1cm length of the plastic coating was removed from both ends of an optical fiber, to avoid interference

#153624 - $15.00 USD Received 31 Aug 2011; revised 14 Oct 2011; accepted 16 Oct 2011; published 27 Oct 2011

from subsequent solvent processing, and then each end was cleaved. One end was affixed to the mount and translated into the resin mould until 50 µm remained between the end face and the bottom surface of the mould. A microscope slide was placed in contact with the bottom of the resin mould and the entire unit was transferred to a hot plate heated to 110 °C. Pieces of vacuum-baked SU-8 were then placed within the mould (Fig. 2B) and allowed to melt and re-flow around the fiber tip (Fig. 2C). The mount was then cooled to room temperature and the cover glass was removed. The resulting mount held an optical fiber embedded to controlled depth in a low-solvent-content 1 to 2mm thick plug of SU-8 resin, ready for fabrication of the micro-structure onto the fiber end-face.

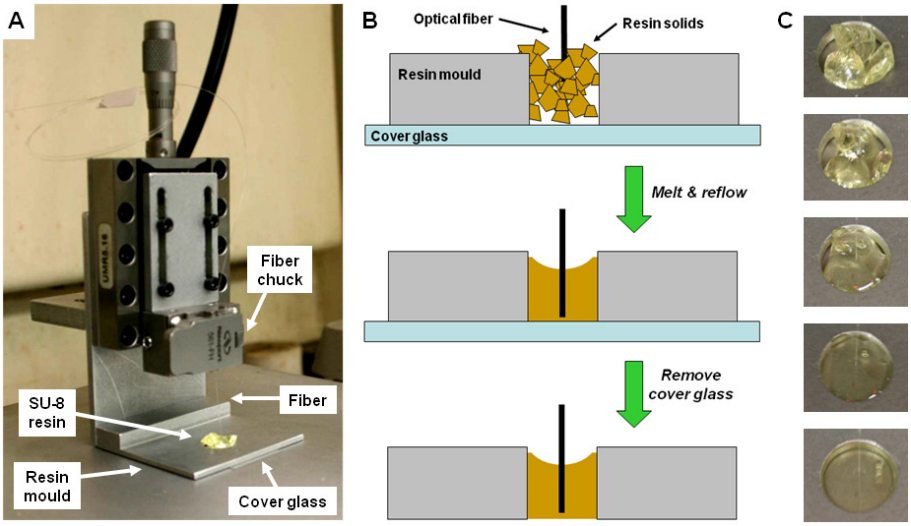


Fig. 2. Melt-reflow processing of SU-8 in preparation for DLW of a micro-structure onto the end-face of an optical fiber. (**A**) Optical fiber and SU-8 resin sample mount. (**B**) Schematic of the melt-reflow process. (**C**) Images of SU-8 melting and reflowing within the resin mould. Upon cooling, the optical fiber becomes embedded at the pre-set depth within the solidified plug of SU-8 resin.

### *2.4. Direct laser writing onto fiber end face*

Figure 3 illustrates schematically the optical configuration used for DLW onto the end-face of optical fibers. It consists of writing-, imaging-, and illumination sub-systems. The writing and imaging sub-systems are similar to those reported previously for typical implementations of DLW [8].

For DLW onto the end-face of a fiber, the fiber mount is affixed to a three-axis piezo-controlled nanopositioner (Physik Instrumente P-563.3CD) supported above the objective of an inverted microscope (Nikon TE2000-U). The output of a continuous wave mode-locked femtosecond laser (Coherent-Mira, 800-nm center wavelength, 120-fs pulse duration, 76 MHz repetition rate) is routed through a shutter, a half-wave plate/polarizer combination, a beam expander, and then into a 100x/1.4 *NA* oil-immersion objective (Nikon) that focuses the writing beam into the resin plug. The average focused power used to create the structures shown in Fig. 1 was 2.4 - 3.0 mW, as measured at the exit aperture of the objective.

The illumination sub-system provides a convenient means for co-locating the write beam with the core of the fiber in both the transverse and axial directions. HeNe laser light coupled into the free end of the fiber emerges from the end-face immersed in resin plug, enabling the core to be imaged with the CCD camera. The fiber mount is then translated until the reflected image of the write beam is coincident with the illuminated core, providing a reference point for fabrication of the target structure.

#153624 - $15.00 USD Received 31 Aug 2011; revised 14 Oct 2011; accepted 16 Oct 2011; published 27 Oct 2011

To photo-pattern a micro-optic, a structure file was first defined for computer controlled exposure. The structure file consists of line segments spaced on a grid in the *xy*-plane and lying parallel to the *z*-axis, where the *z*-axis is parallel the focused laser beam, and likewise normal to the fiber end-face. The exposure and post-exposure processing conditions described here generate polymerized lines having a lateral width of *circa* 0.5 μm. The grid spacing was thus set to $\Delta x = \Delta y = 0.5$ μm, so line segments partially overlapped and fused, creating a solidified internal volume. The sample mount is translated relative to the focal spot at 50 μm/s, as the shutter, attenuator, and nanopositioner are synchronously controlled from the microcomputer according to the structure definition file. Following exposure, samples are baked to activate cross-linking (15 min. at hotplate temperature of 105 °C), transferred to a glass plate and allowed to cool (5 min), immersed in propylene glycol methyl ether acetate to remove unexposed resin, rinsed with methanol, then dried in air, leaving a free-standing micro-structure remaining on the substrate.

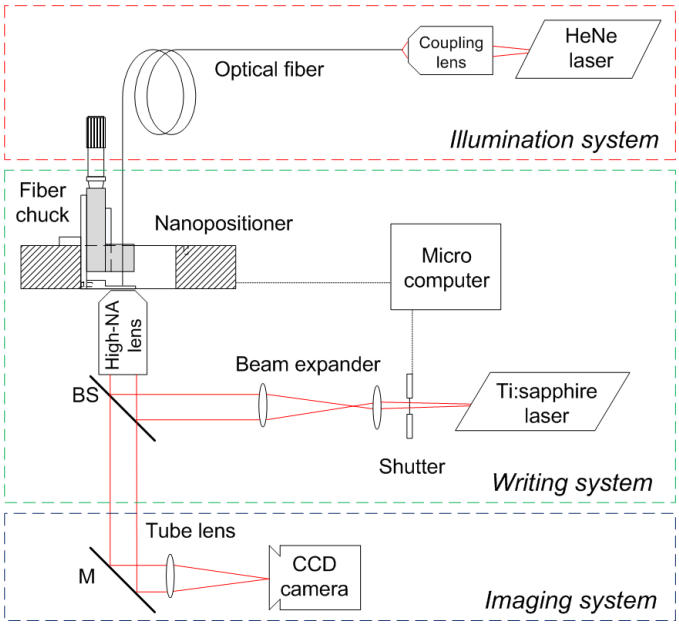


Fig. 3. System for fabricating micro-structures on the end-face of an optical fiber by DLW in SU-8.

### *2.5. Characterization of structures*

Microstructures fabricated on the end-face of an optical fiber were imaged using scanning electron microscopy (SEM). The SEM images provided a means for qualitatively assessing the structure fidelity and quantitatively measuring structural features, such as lens radius of curvature. Side-view images were used to measure relative distance from the substrate (end-face of the fiber) to the curved edge of the lens, and then these data were fit to the equation for a circle to obtain the radius of curvature and the maximum height of the lens above the substrate. The uncertainty in the fitted quantities is estimated to be less than 5%.

Beam spatial irradiance profiles were measured to characterize the performance of some optical fibers bearing microlenses fabricated by DLW in SU-8. Beam parameters derived from these measurements are summarized in Table 1. A HeNe laser was coupled into the optical fiber at the free end, and the beam emerging from the lens-bearing end was imaged at a series of distances *z* from the end-face using a CCD camera mounted on an optical rail. The images were analyzed by measuring irradiance line-profiles passing through the beam centroid and parallel to the *x*- and *y*-axes, fitting the profiles to a Gaussian function, then extracting the full-width at half maximum (FWHM) of the fitted curve. These data were used

#153624 - $15.00 USD Received 31 Aug 2011; revised 14 Oct 2011; accepted 16 Oct 2011; published 27 Oct 2011

to obtain the beam radius and beam divergence angle at the $1/e^2$ point. The fiber bearing the cylindrical lens was oriented prior to measurement with the fast-focusing axis parallel to the $x$-axis. In Table 1, the ellipticity of a beam is quantified by the ratio of the beam FWHM measured along the shortest and longest axes.

### *2.6. Calculation of far-field beam width and divergence*

The propagation of light emerging from microlens-tipped fibers was modeled by $q$transformation of Gaussian beams [9], a paraxial Gaussian beam approximation. For these calculations, $\lambda_0$ = 633 nm, and the refractive index within the fiber and within SU-8 were taken as $n_{core}$ and 1.592 [10], respectively. The $1/e^2$ beam radius immediately at the end-face was estimated as $\omega_0$ = 2.46 μm by iteratively adjusting $\omega_0$ and $q$-transforming the beam until a value was found for which the calculated beam divergence matched that observed from experiment with a bare fiber. Output from a lens-tipped fiber was modeled by beginning with a Gaussian field of beam radius $\omega_0$ at the core and sequentially applying $q$-transformation matrices to account for refraction at the fiber/SU-8 interface, propagation through the base of the SU-8 lens, refraction at the curved surface of SU-8/air interface, and finally propagation through air to a given distance measured from the fiber end-face.

**Table 1. Optical characteristics of microlenses fabricated on the end-face of a single-mode fiber by DLW in SU-8 and the far-field beams generated when light having $\lambda_0$ = 633 nm exits the lens-tipped end.**

| | **Bare Fiber** | **34.1 μm PC Lens** | **18.3 μm PC Lens** | **15.7 μm CYL Lens** | |
|---|---|---|---|---|---|
| Microlens parameters | | | | | |
| $R$, observed | -- | 34.1 μm | 18.3 μm | 15.7 μm | |
| $R$, targeted | -- | 40.0 μm | 20.0 μm | 10.8 μm | |
| Peak-height of lens | -- | 4.3 μm | 9.4 μm | 3.8 μm | |
| Beam width, $z$ = 15 mm | | | | ***Fast axis*** | ***Slow axis*** |
| Observed FWHM | 1.44 mm | 1.76 mm | 2.07 mm | 2.30 mm | 1.64 mm |
| Calculated FWHM | -- | 1.57 mm | 1.82 mm | 2.10 mm | -- |
| Observed $1/e^2$ | 1.23 mm | 1.49 mm | 1.76 mm | 1.95 mm | 1.40 mm |
| Calculated $1/e^2$ | -- | 1.33 mm | 1.55 mm | 1.79 mm | -- |
| Divergence angle | | | | | |
| Observed | 0.082 rad | 0.099 rad | 0.12 rad | 0.13 rad | 0.093 rad |
| Calculated | -- | 0.088 rad | 0.10 rad | 0.12 rad | -- |
| Beam ellipticity | 1.03 | 1.02 | 1.02 | 1.02 | |

"PC" indicates a plano-convex lens. "CYL" indicates a cylindrical lens. Parameters for a bare single-mode fiber are included for comparison. The values of beam width reported for PC-lens-tipped fibers are an average of that measured along the $x$- and $y$-axes. The beam ellipticity is expressed as the ratio of the FWHM measured along the orthogonal axes. Calculated beam widths and divergence were determined by $q$-transformation of Gaussian beams [9], as detailed in Section 2.6.

## 3. Results and discussion

### *3.1. Processing and micro-structure fabrication*

The structures prepared by the method described here include simple plano-convex lenses, a cylindrical lens, a compound lens system, and a woodpile photonic crystal structure. Plano-convex lenses were prepared with a targeted radial curvature of $R$ = +20 μm (Fig. 1A) and $R$ = +40 μm (not shown). The actual structures were found to have lens curvatures of $R$ = +18.3 μm and $R$ = +34.7 μm, respectively. The compound lens system was fabricated with targeted positive- and negative-lens curvatures of $R$ = +34 μm and $R$ = −20 μm. The actual curvatures were found to be $R$ = +29.5 μm and −23.1 μm. Differences in curvature between the targeted

#153624 - $15.00 USD Received 31 Aug 2011; revised 14 Oct 2011; accepted 16 Oct 2011; published 27 Oct 2011

and actual structures are thought to result primarily from resin re-flow occurring during the post-exposure bake, which could be reduced by optimizing the post-exposure process. Although the fidelity of the fabrication was not optimized, we found that the optical performance was reproducible when a given structure was fabricated multiple times, as discussed below.

Viewing down onto the end face of the optical fiber (Fig. 1A) confirms that the micro-optics can be fabricated well centered with respect to the fiber, and thus well overlapped with the core. Side views of the cylindrical lens (Figs. 1D - 1E) show that the serial patterning process enables the radius of curvature along the fast and slow (non-focusing) axes to be defined independently. Additionally, by simply rotating the coordinates of the structure file, the orientation of these axes could be set with respect to those of a radially anisotropic surface, such as a polarization-preserving fiber.

The compound-lens structure was created in a single serial exposure by patterning the smaller plano-concave optic in contact with the fiber end-face and the plano-convex optic suspended by four supports, so the two lenses are separated by an air-gap. Figures 1F - 1H show a variant of this device that was created with quadrants one and three of the negative lens purposefully omitted so its concavity would be clearly visible. The length of the supports could be altered to vary the separation between the micro-optics and thereby vary their collective focusing properties. The woodpile structure (Figs. 1I - 1K) provides an extreme example of how the method can be used to create new integrated photonic devices consisting of micro-optical structures with a high degree of undercut and topological complexity. Collectively, these examples illustrate the power of this method for creating truly three-dimensional structures in SU-8 directly on the end-face of an optical fiber.

During the melt-reflow process itself, the optical fiber shifts laterally as the molten resin flows around the fiber. Air bubbles can also form within the resin as it fuses and traps air (Fig. 2C). Bubble formation and air trapping can be minimized by selecting large pieces for melt-reflow. Ten minutes of melt-reflow proved sufficient for bubbles to migrate to the surface and burst, for the resin meniscus to settle to its final shape, and for the fiber to relax to a vertical position within the resin plug. The overall process typically required no more than 30 minutes to prepare a sample. Because the resin solidifies around the optical fiber, it cannot move during photo-patterning, as is the case for liquid-resin approaches [3,4], so the method reported here provides an inherent advantage for precision micro-fabrication onto optical fibers.

### *3.2. Characterization and performance of vacuum-baked resin*

$^{1}$H NMR analysis showed that the solvent content of SU-8 2075 resin as supplied was 19 mass-percent. The solvent content dropped rapidly with heating *in vacuo* and could be reduced to nearly one mass-percent in as little as one hour. Significantly longer heating was needed to reduce the solvent content further, as the molten, low-solvent resin is highly viscous. A solvent content of 0.68 mass-percent was achieved with overnight heating (14 hours).

The woodpile structure proved useful for evaluating the fabrication process and how solvent content and other parameters affect structure fidelity. This particular structure is intricate, having features with sizes on the order of a micron, so it will not be self-supporting if the degree of cross-linking, and consequently the mechanical robustness, are poor. Figure 4 shows SEM images of woodpile structures prepared by DLW using vacuum-baked resin heated for one, three, and fourteen hours, and viewed normal to the supporting substrate. The highest quality structure is obtained when prepared using resin-solids heated for 14 hours. In that case, the feature-edge contrast is high, the features are least rounded, the interior of the structure is least filled in, and the crossing points of overlapping “logs” are most sharply defined. This suggests that low solvent content helps confine the polymerization reaction and thus improves the patterned structure integrity, possibly by limiting acid diffusion or resin reflow that can occur during the post-exposure bake. These observations are consistent with earlier reports of how solvent content affects performance of liquid SU-8 resin that is spin

#153624 - $15.00 USD Received 31 Aug 2011; revised 14 Oct 2011; accepted 16 Oct 2011; published 27 Oct 2011

coated and soft-baked in the customary way for DLW, conventional photo-lithography, X-ray, or e-beam patterning of micro- and nano-scale devices [11–16].

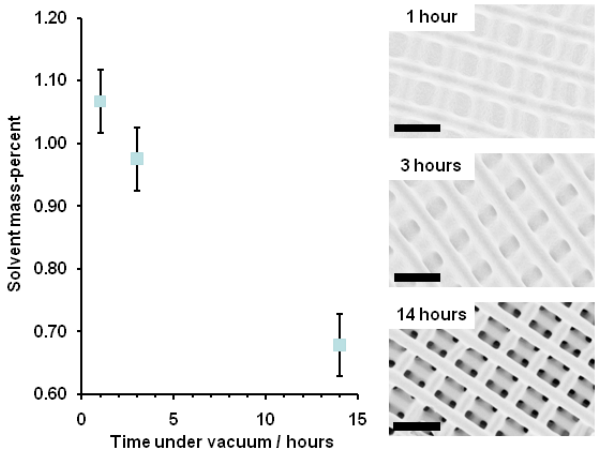


Fig. 4. Effect of residual solvent on the fidelity of woodpile structures created by DLW in SU-8 on the end-face of an optical fiber. (***Left***) Graph of solvent mass-percent versus time for which the resin was heated *in vacuo*. (***Right***) Top-view SEM images of woodpile structures prepared by DLW using resin solids heated *in vacuo* for the specified time. All scale bars correspond to 5 μm.

We examined the possibility of dispensing SU-8 2075 as a liquid directly into the sample mould and around the pre-hung fiber and then baking the sample mount to drive off solvent. This did yield a solid resin plug with good optical quality. But DLW experiments produced poorly defined structures with low structural integrity that did not survive the developing step. $^1$H NMR analysis showed that the solvent content of the resin plug produced in this way remained high, generally above five mass-percent, even with protracted periods of baking, up to 24 hours at 110 °C. We reason that solvent evaporation is hindered by the restricted volume, low exposed surface area, and comparatively large thickness of the resin droplet, leaving the melt-reflow process as the preferred approach. Other investigators have encountered similar difficulty when attempting to fabricate in ultra-thick (~1 mm) slabs of SU-8 cast from the liquid resin [13,17,18]. Becnel and associates conclude that a low-solvent skin forms at the resin-air interface during the pre-exposure bake that hinders solvent release from the underlying bulk. Various approaches have been proposed for surmounting this problem, including a multi-layer casting and "dry chip casting" [17]. Denning and associates used a "hot-casting" approach to study shrinkage of specially formulated SU-8 from which low-molecular-weight fractions of the epoxide oligomer had been removed [16]. These casting methods are similar to the melt-reflow approach discussed in the present work.

### *3.3. Optical characterization*

Figure 5 shows examples of beam profiles imaged at selected distances $z$ from the end-face of an optical fiber bearing an $R = +18.3$ μm plano-convex lens. Images like these were used to obtain measurements of the beam width along the $x$- and $y$-axes as a function of distance $z$ for several micro-optic-tipped fibers, and these data are plotted in Fig. 6. Relevant beam parameters obtained from these measurements are summarized in Table 1.

From Fig. 6 it is clear that positive-curvature microlenses cause the exiting beam to diverge more quickly than that from the bare fiber. Additionally, Table 1 shows that the divergence angle increases as the focusing power of the lens increases. The largest divergence is observed in the spread of the beam parallel to the fast-focusing axis of the cylindrical lens, which has the smallest radius of curvature. The beam divergence along the "slow-axis" (non-focusing) is closest to that of the bare fiber, as expected. These observations suggest these microlenses bring the exiting beam to a focus near the end face, after which the beam diverges

#153624 - $15.00 USD Received 31 Aug 2011; revised 14 Oct 2011; accepted 16 Oct 2011; published 27 Oct 2011

producing an overall beam spread that exceeds that of the bare fiber. The same behavior was predicted by simulations of the beam width versus distance from the fiber end-face. Calculated values for the beam width and divergence angle listed in Table 1 exhibit the same trend and are in good agreement with those observed experimentally.

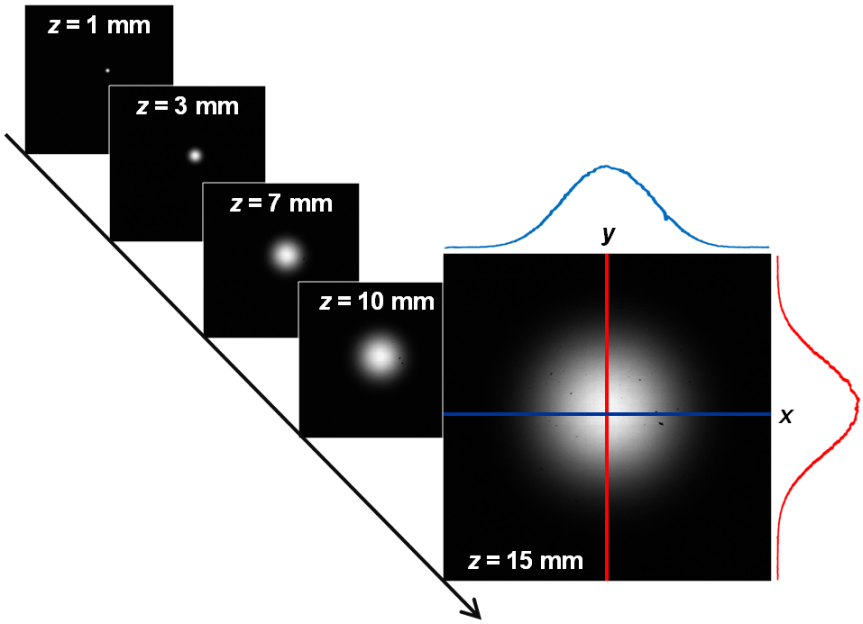


Fig. 5. Example beam profiles, obtained at selected distances $z$ from the end-face of an optical fiber bearing an $R$ = +18.3 μm plano-convex lens. Irradiance line-profiles like that shown for $z$ = 15 were measured along the $x$- and $y$-axes and through the centroid to obtain the FWHM of the beam.

Lee and Barnes used conventional lithography to create hemispherical microlenses on the end of single-mode fibers and experimentally characterized their focusing [19]. Lee modeled the focusing using the paraxial Gaussian beam approximation (as applied in this work), and compared the results to those obtained using Frensel diffraction theory [20]. It was found that the position of maximum intensity and the position of minimum beam size differ by less than 10% from those predicted with paraxial theory when the ratio of the lens radius to beam size at the fiber end-face, $r_0/\omega_0$, is 1.65 and 1.8, respectively. Additionally, values calculated with both levels of theory for a given focusing parameter converge for $r_0/\omega_0 > 3$. Given that $r_0/\omega_0 > 5$ in the present work, use of the paraxial theory is satisfactory, and it cannot be the source of difference observed between calculated and experimental beam parameters. Lee also showed that lens aberration impacts the focusing parameters significantly more than the level of theory used to describe them. Consequently, the differences observed in this work between theory and experiment are most likely due to imperfection in the microlens shape.

Given that the internal volume and surface of the micro-optics are defined by photo-exposure along an array of lines, one might expect they would be partially diffractive or highly scattering. Close inspection of the microstructures shown in Fig. 1 reveals that their surfaces are in fact smooth on the micron length-scale. Additionally, the beam profiles in Fig. 5 show that the microlenses controllably refract the beam without introducing significant scatter. Good surface smoothness was achieved in part by purposefully patterning the micro-optics using *vertically* oriented lines. The terminus of each line could be defined to within 5 nm (the bi-directional repeatability of the nanopositioner), so this together with the line pitch of 0.5 μm enables the optical surface to be defined smoothly. The surface is further smoothed by volumetric overlap of the exposed lines and lateral diffusion of the photoacid and/or polymerization front [17]. Evidently, these effects sufficiently homogenize the internal

#153624 - $15.00 USD Received 31 Aug 2011; revised 14 Oct 2011; accepted 16 Oct 2011; published 27 Oct 2011

volume of the micro-optics that far-field diffraction is not observed. Diffusion is generally the bane of the photolithographer. But in the application demonstrated here, diffusion appears to contribute to the process and improve performance of the micro-optical devices. To the best of our knowledge, this aspect of DLW has not been discussed previously.

Figure 6 shows that within experimental error the beam widths along the *x*- and *y*-axes are the same at a given distance, for either a bare fiber or one supporting a plano-convex lens. Consequently, the axial ratios for these fibers are nearly unity (Table 1). This is as would be expected for linearly polarized light focused by a radially symmetric lens having low numerical aperture [21]. In contrast, for the fiber bearing a cylindrical lens, the beam widths along the *x*- and *y*-axes are markedly different. The beam width associated with the non-focusing axis is close to that obtained from the bare fiber, whereas the beam width along the fast-focusing axis is 40% larger, and the axial ratio is significantly larger than unity. These observations are consistent with expectations for focusing through a cylindrical lens, and it illustrates how an SU-8 micro-optic created by DLW can be used to transform the output of an optical fiber significantly.

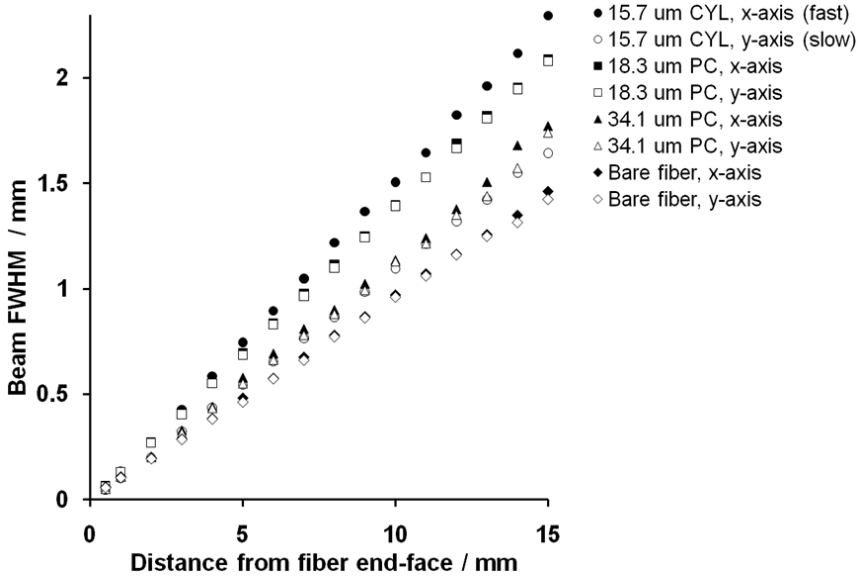


Fig. 6. Beam width versus distance, *z*, from the end face of optical fibers bearing refractive lenses created by multi-photon direct laser writing in SU-8. The label "CYL" indicates a cylindrical lens, whereas "PC" indicates a plano-convex lens. Values preceding these labels specify the lens radius of curvature in microns. Beam width measurements for a bare fiber are included for comparison. Measurements made parallel to the *x*- and *y*-axes are represented by filled and hollow symbols, respectively.

To explore the reproducibility in optical performance that can be achieved using this method, a plano-convex lens having a targeted curvature of $R = +20$ μm was fabricated onto three separate optical fibers, and then for each the output beam widths (FWHM) along the *x*- and *y*-axes were measured and compared. The plot in Fig. 7 shows that the beam widths measured along the *x*-axis nearly overlap for all three fabrications. At $z = 15$ mm specifically, the beam widths along the *x*-axis were 2.09 mm, 2.09 mm, 2.10 mm, and the mean width was 2.09 mm. The corresponding widths along the *y*-axis were 2.08 mm, 1.99 mm, 2.08 mm, and the mean width was 2.05 mm. From these values one can calculate the maximum percent-difference in beam-width observed along the *x*- and *y*-axes as −0.5% and + 2.9%, respectively. These data suggest that high reproducibility in optical performance can be achieved with this method.

#153624 - $15.00 USD Received 31 Aug 2011; revised 14 Oct 2011; accepted 16 Oct 2011; published 27 Oct 2011

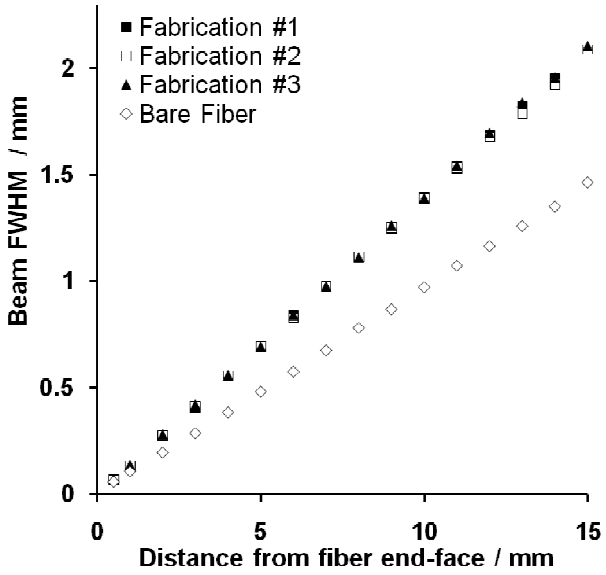


Fig. 7. Reproducibility in optical performance observed for three separate fabrications of a plano-convex lens (targeted curvature $R$ = +20 μm) onto the end face of an optical fiber by multi-photon direct laser writing in SU-8. Beam width measured parallel to the $x$-axis is plotted versus distance $z$ from the end face of the fiber. Measurements obtained for a bare fiber are included for comparison.

## 4. Conclusion

An approach has been demonstrated for fabricating micro-structures onto the end-face of an optical fiber using multi-photon DLW in the high-performance resist SU-8. A compound lens and a woodpile photonic crystal were prepared to illustrate how the method can be used to integrate directly onto a fiber truly three-dimensional structures with a high degree of undercut and complex topology that would be difficult or impossible to create by other approaches. Optical characterization of the refractive lens devices shows that low scatter and high reproducibility are attainable. Further development of this approach could doubtless yield additional improvements in fabrication fidelity, tolerance, and optical performance. Improving the post-exposure process and refining the fiber mount are avenues for further exploration.

The method described here offers potential for rapid fabrication of fiber-tipped devices. For example, the lens shown in Fig. 1A requires only four minutes to photo-pattern. Preparing the sample and post-exposure baking require considerably more time. But these portions of the process could be parallelized. With further engineering, a more sophisticated mount could be created that enables multiple fibers to be bundled and processed in parallel. Photo-exposure per fiber could remain a serial process, whereas pre- and post-exposure processing would be done in parallel, greatly accelerating throughput. If we consider then just the photo-exposure time, and assume continuous fabrication, 10,000 devices like that in Fig. 1A could be made in approximately 30 days.

The technique opens a route to more complex integrated photonic devices that leverage the technology of fiber optics. High efficiency optical fiber couplers, low insertion-loss micro-laser couplers, fiber output beam shapers, and a new class of optical sensors could be realized. Fabrication of novel beam coupling devices could be a particularly fruitful application. The method could be used to create aspherics, radially asymmetric lenses, or multi-lens elements that enable more efficient fiber-coupling from sources that generate irregular beams, like laser diodes or vertical-cavity surface emitting lasers. A new class of integrated photonic devices, particularly sensors, could be realized with collective

#153624 - $15.00 USD Received 31 Aug 2011; revised 14 Oct 2011; accepted 16 Oct 2011; published 27 Oct 2011

performance that was previously unachievable, including high immunity from electromagnetic interference, chemically inertness, and the potential to operate in extreme environments interfaced electro-optically to remote driving electronics.

**Acknowledgements**

This work was supported by NSF CAREER grant 0748712. D. J. Freppon has been partially supported by NSF grants 0525429 and 0806931. The authors are grateful to the referees for their thoughtful evaluation of the manuscript and their many constructive comments.

#153624 - $15.00 USD Received 31 Aug 2011; revised 14 Oct 2011; accepted 16 Oct 2011; published 27 Oct 2011